Atmospheric Tides

J Oberheide, Clemson University, Clemson, SC, USA
ME Hagan and AD Richmond, National Center for Atmospheric Research, Boulder, CO, USA
JM Forbes, University of Colorado, Boulder, CO, USA

This article is a revision of the previous edition article by M Hagan, J Forbes, A Richmond, volume 1, pp 159–165, © 2003, Elsevier Ltd.

Synopsis

Atmospheric tides are planetary-scale wave motions in the neutral atmosphere with periods defined by Earth's rotation rate. They are among the most striking dynamical features in the mesosphere and thermosphere, and are known to redistribute ionospheric plasma through dynamo processes. This article reviews the salient features of the tides from theoretical and observational perspectives, including the recent discovery that atmospheric tides connect planetary-scale weather patterns with the 'space weather' of the ionosphere-thermosphere.

Introduction

Atmospheric tides are ubiquitous features of the Earth's atmosphere. They are the persistent global oscillations that are observed in all types of atmospheric fields, including wind, temperature, pressure, density, and geopotential height. Tidal oscillations have periods that are some integer fraction of a solar or lunar day. The solar diurnal and semidiurnal tides have 24 and 12 h periods, respectively. The lunar diurnal tidal period is about 24.8 h, while the lunar semidiurnal period is 12.4 h. Scientists often use a shorthand notation to represent solar and lunar tides. S1 and S2 refer respectively to the solar diurnal and semidiurnal tides. Their lunar counterparts are M1 and M2.

Atmospheric tides have been studied for many years, since they are evident in both surface pressure and magnetic observations that date back to the early part of the twentieth century. Figure 1 illustrates a time series of surface pressure measurements made at Batavia (now known as Jakarta, Indonesia) during the first 5 days of January in 1925. The dominant feature of this time series provides evidence of the solar semidiurnal atmospheric tide. Specifically, there is a 1 to 2-hPa deviation from the average pressure of about 1011 hPa that occurs regularly at 12 h intervals. This semidiurnal variation is modulated by other variations, but the former is such a persistent oscillation that the semidiurnal tide is also the dominant oscillation in monthly, yearly, and even multiyear averages of daily surface pressure measurements made at Batavia.

Atmospheric tides are further characterized by their sources. The Moon's gravity forces the lunar atmospheric tide, while solar atmospheric tides can be excited in several ways, including the absorption of solar radiation, large-scale latent heat release associated with deep convective clouds in the troposphere, the gravitational pull of the Sun, and as secondary waves due to nonlinear wave–wave interactions. The restoring force that acts on atmospheric tides is gravity, so tides are a special class of buoyancy or gravity waves. Unlike high-frequency gravity waves, tides are affected by the Earth's rotation and sphericity because of their comparatively large periodicities and horizontal scales. Solar atmospheric tides are generally larger than lunar tides and dominate the tidal motions in the middle and upper atmosphere, that is, the stratosphere, mesosphere, and thermosphere. Movie 1 illustrates the combined diurnal and semidiurnal tidal motions caused by solar atmospheric tides in the lower thermosphere. Temperature and wind speeds can vary by more than 60 K and >100 m s^{-1} within a few hours.

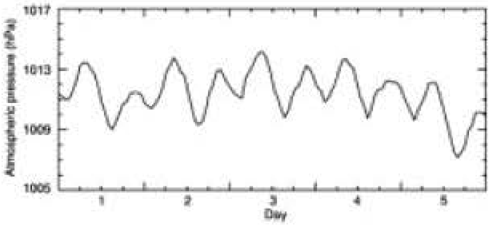

Figure 1 Surface pressure (hPa) at Batavia (Jakarta, Indonesia) against time during the first 5 days of January 1925.

The general mathematical expression for a tidal oscillation is given by eqn [1], where A is the magnitude of the variation in some atmospheric field, σ is its frequency, t is universal time, λ is longitude, and $s \geq 0$ is the zonal wavenumber (the number of wave crests that occur along a latitude circle). The $(s\lambda - \sigma t)$ form of eqn [1] is chosen so that the sign of σ is indicative of the zonal direction of propagation: $\sigma > 0$ corresponds to eastward propagating waves and $\sigma < 0$ to westward propagating waves. φ is the so-called tidal phase. A crest of the wave occurs when eqn [2] is satisfied.

$$A\cos(s\lambda - \sigma t - \varphi) \qquad [1]$$

$$\varphi = s\lambda - \sigma t \qquad [2]$$

The horizontal phase speed of the tide, c_{ph}, is defined by differentiating eqn [2] (eqns [3] and [4]).

$$s\,\mathrm{d}\lambda - \sigma\,\mathrm{d}t = 0 \qquad [3]$$

$$c_{\mathrm{ph}} \equiv \frac{\mathrm{d}\lambda}{\mathrm{d}t} = \frac{\sigma}{s} \qquad [4]$$

For solar tides, the mth harmonic frequency is $\sigma_m = m\sigma_1$, where m is a positive or negative integer and $\sigma_1 = (2\pi/24)\ \mathrm{h}^{-1}$. Rewriting the mathematical expression for a tide in terms of LT (hours), $t_L = t + \lambda/\sigma_1$, results in a mathematical expression of the form of eqn [5].

http://dx.doi.org/10.1016/B978-0-12-382225-3.00409-6

$$A\cos((s+m)\lambda - \sigma_m t_L - \varphi) \qquad [5]$$

For the subset of atmospheric tides known as migrating solar tides, $s = -m$ (with $m < 0$) and eqn [5] reduces to eqn [6].

$$A\cos(|m|\sigma_1 t_L - \varphi) \qquad [6]$$

Thus, migrating solar tides have the same local time variation at all longitudes. If $m = -1$ and $s = 1$, the tide is diurnal and moves or migrates westward in longitude with the apparent motion of the Sun from the perspective of a ground-based observer. Further, $c_{ph} = -(2\pi/24)\ h^{-1}$. Similarly, if $m = -2$ and $s = 2$, then the wave is a migrating semidiurnal tide. The remaining set of global-scale waves with tidal periods that are not Sun-synchronous are known as nonmigrating tides. Nonmigrating tides may be viewed as waves that propagate to the west more rapidly or slowly than the Sun, or that propagate eastward, or that are standing. Migrating and nonmigrating solar tides are often identified by using a letter/number code that indicates frequency, propagation direction, and zonal wavenumber: DWs or DEs is a westward or eastward propagating diurnal tide, respectively, with positive zonal wavenumber s. For semidiurnal tides, D is replaced by S, and D0, S0 are standing diurnal and semidiurnal tides, respectively. With this nomenclature, the migrating diurnal (semidiurnal) tide is DW1 (SW2) and DE3, for example, is an eastward propagating diurnal tide of zonal wavenumber 3.

All tides contain components that propagate in the vertical direction z. The effects of upward-propagating tidal components are particularly important because these waves grow in amplitude $\sim\exp(z/2H)$ with scale height H ($= k_B T/Mg$ where k_B is the Boltzmann constant, T is temperature, M is the mean molecular mass, and g is Earth's gravity acceleration) as they conserve energy in an atmosphere whose density decreases with increasing altitude. Thus, tides with insignificant amplitudes in their lower atmospheric regions of excitation often affect the upper atmosphere profoundly because they introduce large atmospheric variations with local time and because they may dissipate and deposit their energy and momentum therein.

Classical Tidal Theory

Classical tidal theory treats the tides as perturbations on a basic state with neither mean-flow nor horizontal temperature gradients in an inviscid atmosphere. It provides a reasonable description of atmospheric tides in the lower and middle atmosphere, including the mesosphere and is therefore quite useful to demonstrate important tidal characteristics. As described in detail by Chapman and Lindzen (1970), the linearized primitive equations (Dynamical Meteorology: Primitive Equations) for wave motions described by eqn [1] and given (s, σ) can be reduced to a single equation for, for example, geopotential. The resulting equation is separable in its latitude and altitude dependence. The latitudinal part is described by Laplace's tidal equation and solved by a complete orthogonal set of eigenfunctions (called Hough modes) and eigenvalues or separation constants (called equivalent depths).

Each Hough mode $\Theta_n^{s,\sigma}$ is a series of associated Legendre polynomials with $|n| \geq s$ being the so-called meridional index because it provides information on the number of latitudinal nodes and symmetry characteristics. It is quite common to refer to a specific Hough mode as the Θ_n^s mode or simply the (s,n) mode and to provide the frequency information externally. The equivalent depth $h_n^{s,\sigma}$ determines the vertical structure of each Hough mode because it is linked to the vertical wavelength λ_z (eqn [7]).

$$\lambda_{z,n}^{s,\sigma} = \frac{2\pi H}{\sqrt{\frac{\left(\kappa H + \frac{dH}{dx}\right)}{h_n^{s,\sigma}} - \frac{1}{4}}} \qquad [7]$$

with scale height H, $\kappa = (\gamma - 1)/\gamma$ and adiabatic index $\gamma = 7/5$, and normalized height $x = z/H$. Equation [7] implies that equivalent depths must be positive but smaller than roughly 8 km for vertical wave propagation. Larger values or negative equivalent depths imply vertically trapped modes. Figure 2 illustrates Hough modes corresponding to the first two propagating and trapped modes of the migrating DW1 and nonmigrating DE3 tides, respectively. Diurnal propagating modes generally maximize at low to middle latitudes and trapped modes at middle to high latitudes.

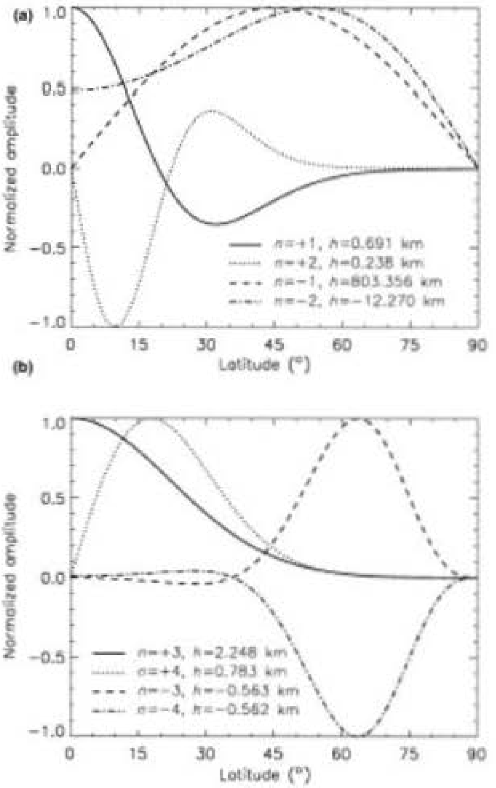

Figure 2 (a) Hough modes for the migrating diurnal solar tide (DW1). The meridional index n is positive for propagating tides and negative for trapped tides. (b) Same as (a) but for the DE3 nonmigrating tide.

Symmetric Hough functions are mirror images about the equator and occur if $n+s$ is even (odd) for positive (negative) values of n. Antisymmetric modes change sign at the equator and occur if $n+s$ is odd (even) for positive (negative) n. Tidal variations δF in temperature, pressure, geopotential, density, and vertical wind as function of normalized height x, latitude ϑ, zonal wavenumber s, and frequency σ are described by eqn [8]

$$\delta F^{s,\sigma}(x,\vartheta) = \sum_n \delta F_n^{s,\sigma}(x)\Theta_n^{s,\sigma}(\vartheta) \qquad [8]$$

Zonal (u) and meridional (v) wind variations are described by eqns [9] and [10],

$$\delta u^{s,\sigma}(x,\vartheta) = \sum_n \delta u_n^{s,\sigma}(x)U_n^{s,\sigma}(\vartheta) \qquad [9]$$

$$\delta v^{s,\sigma}(x,\vartheta) = \sum_n \delta v_n^{s,\sigma}(x)V_n^{s,\sigma}(\vartheta) \qquad [10]$$

with the wind expansion functions shown in Figure 3 (eqns [11] and [12])

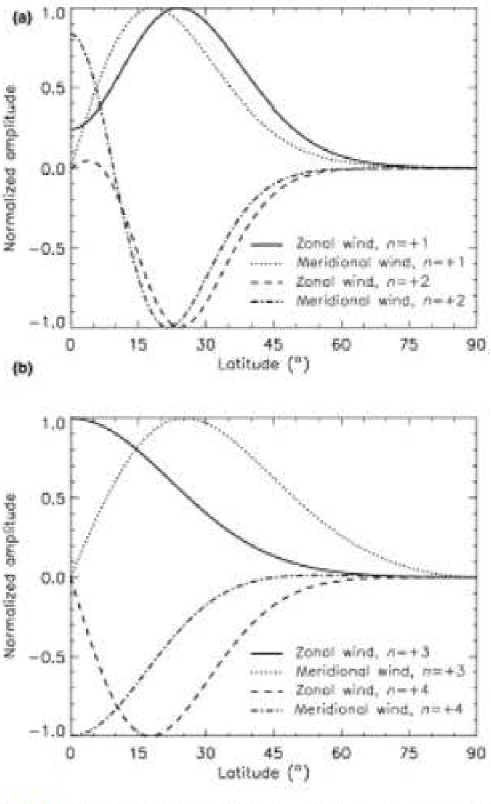

Figure 3 (a) Wind expansion functions for the migrating diurnal solar tide (DW1). The first two propagating modes are shown. (b) Same as (a) but for the DE3 nonmigrating tide.

$$U_n^{s,\sigma}(\vartheta) = \frac{1}{(f^2-\sin^2\vartheta)}\left[\frac{s}{\cos\vartheta}+\frac{\sin\vartheta}{f}\frac{\mathrm{d}}{\mathrm{d}\vartheta}\right]\Theta_n^{s,\sigma}(\vartheta) \qquad [11]$$

$$V_n^{s,\sigma}(\vartheta) = \frac{1}{(f^2-\sin^2\vartheta)}\left[\frac{s\tan\vartheta}{f}+\frac{\mathrm{d}}{\mathrm{d}\vartheta}\right]\Theta_n^{s,\sigma}(\vartheta) \qquad [12]$$

with $f=\sigma/(2\Omega)$ and Earth's angular velocity Ω. The zonal wind expansion functions $U_n^{s,\sigma}$ have the same symmetry as the corresponding Hough modes. $V_n^{s,\sigma}$ on the other hand are symmetric (antisymmetric) when the corresponding Hough modes are antisymmetic (symmetric).

The classical tidal theory approximates the tidal motions in the lower and middle atmosphere reasonably well, including the mesosphere. Classical methods of computing tides, however, do not work when mean zonal winds or dissipation are included, because the mathematical solutions become inseparable in the latitudinal and vertical coordinates. Hough modes are no longer eigenfunctions of the system and numerical solutions are needed. This is particularly important in the thermosphere where the tides undergo a substantial change in their modal structure when molecular dissipation becomes important. This transition height occurs approximately where the dissipative time scale equals the scale height divided by the vertical group velocity. Amplitudes and phases relax to approximately constant values in the thermosphere and the damping significantly broadens the horizontal structure. It should also be noted that the time constants of eddy and molecular diffusion are proportional to the square of λ_z. Short vertical wavelength tides or modes therefore dissipate more rapidly and cannot propagate into the thermosphere at all.

Migrating Solar Tides

The absorption of radiation by a longitudinally invariant atmosphere is the primary source of migrating solar tides. Owing to the rotation of the Earth, this absorption is periodic in time from the perspective of the ground-based observer. The resultant heating gives rise to migrating tidal oscillations. Solar radiation is absorbed throughout the Earth's atmosphere, thereby exciting migrating solar tides at almost all altitudes. Atomic oxygen, which is the most abundant atmospheric constituent at altitudes about 150 km above the Earth's surface, absorbs the shortest-wavelength solar radiation, known as the extreme ultraviolet. Increasingly longer wavelengths are absorbed as the solar radiation approaches the Earth's surface. Molecular oxygen (O_2) absorbs the far-ultraviolet radiation (100–200 nm) at altitudes near about 100–150 km, and ozone (O_3) absorbs the 200 to 300-nm solar ultraviolet radiation at middle atmospheric altitudes between about 30 and 70 km. Solar infrared radiation may be absorbed by water vapor (H_2O) in the lowest part of the atmosphere.

Even though there is little, if any, tidal forcing due to solar heating in the upper mesosphere (~80–100 km), measurements of winds and temperatures exhibit strong tidal signatures in this region. Figure 4 illustrates an example of the magnitude of the mean winds and the tidal oscillations over Adelaide, Australia, at these altitudes. The data points represent the eastward winds that were measured with the Buckland Park radar during 2 days in August 1994. The dashed curves

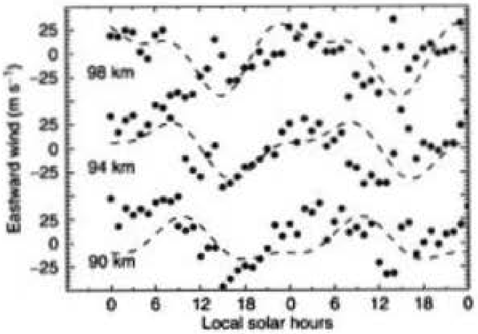

Figure 4 Eastward winds (m s^{-1}) over Adelaide, Australia, against local time (h) on 8–9 August 1994 at 98 km (top), 94 km (middle), and 90 km (bottom). Data points are radar measurements and dashed curves are model predictions that include the migrating diurnal and semidiurnal tidal components. Professor R.A. Vincent provided the Adelaide radar data.

illustrate global-scale wave model (GSWM) tidal predictions for August at the location of Adelaide. While the GSWM differs from the measurements in detail, the model captures the salient features of the observed winds, particularly on 8 August. Differences may be attributable to small-scale waves that are not included in GSWM or to sources of day-to-day tidal variability that are also omitted.

The GSWM predictions include mean winds (17–18 m s^{-1}) and both migrating diurnal and semidiurnal components. Notably, the migrating diurnal amplitudes (20–30 m s^{-1}) are larger than the mean winds. The GSWM diurnal tidal amplitudes are at least a factor of 2 larger than the semidiurnal amplitudes (8–15 m s^{-1}) and the phases of both components shift to earlier times with increasing altitude between 90 and 98 km. This behavior, which is known as downward phase progression, is indicative of upward-propagating wave energy. There are clear signatures of downward phase progression in the GSWM predictions in Figure 4. That is, the wind predictions are most westward near 15.00 h at 98 km and there are similar features at progressively later times and progressively lower altitudes. The vertical wavelength of the migrating diurnal tide over Adelaide is much shorter than that of the migrating semidiurnal tide, so the phase of the former progresses far more rapidly than the phase of the latter and their combined effects result in a pattern of wave maxima and minima that evolves between altitudes.

The migrating diurnal tide below the mesopause (i.e., the region between the mesosphere and thermosphere) originates primarily in the troposphere. Although tropospheric semidiurnal forcing is nonnegligible, there is comparatively more semidiurnal forcing in the middle atmosphere. Thus, the diurnal tidal growth occurs over a deeper altitude region than the semidiurnal growth and it is reasonable to anticipate a diurnal amplitude that is larger than the semidiurnal amplitude in the upper mesosphere. The aggregate characteristics of the mean winds and tides that are illustrated in Figure 4 support the claim that upward-propagating migrating tides govern the large-scale dynamics of the upper mesosphere.

Migrating tides exhibit somewhat complicated behavior in that the latitudinal structure of the horizontal wind oscillations is dramatically different from the temperature, pressure, or vertical velocity structure. For example, the upward-propagating migrating diurnal tide DW1 is characterized by a primary temperature amplitude maximum over the Equator with secondary maxima near ±30°. The horizontal wind amplitudes (Movie 2) exhibit minima over the Equator and nearly symmetric amplitude peaks at low to middle latitudes (±(20–30°)). While ground-based observations provide an important perspective on the local behavior of waves with tidal frequencies, it is impossible to decipher global structures from local structures without conducting correlative analysis of measurements made at multiple locations over a broad range of latitudes. Further, in order to distinguish migrating from nonmigrating tidal components, it is necessary to have a longitudinal distribution of measurements.

The upward-propagating migrating tides dissipate in the lower thermosphere and their contribution to upper thermosphere variability is comparatively small. However, the longitudinally invariant absorption of solar far and extreme ultraviolet radiation efficiently forces a large *in situ* component of the migrating tides that dramatically changes the temperature, density, and wind structure in the upper thermosphere. Figure 5 illustrates its magnitude based on the output from the NRLMSISE-00 (i.e., the 2000 version of the Naval Research Laboratory Mass Spectrometer Incoherent Scatter Radar Extended) empirical model. Local time mass density variations at 12:00 Universal Time are on the order of a factor of 3 when the tides (diurnal, semidiurnal, terdiurnal) are included (left panel) but almost nonexistent when the

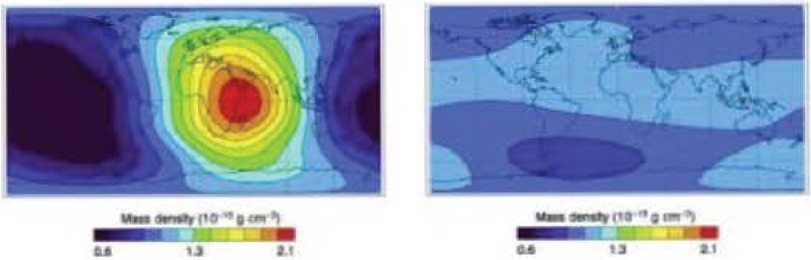

Figure 5 Global distribution of neutral mass density at 12:00 Universal Time and 400 km altitude on 21 September 2010 with (left) and without (right) thermospheric tides. Data shown are from the NRLMSISE-00 model and do not include nonmigrating tides.

tides are excluded (right panel). The largest tidal signal in Figure 5 (left panel) comes from the migrating diurnal tide DW1. It maximizes at the equator (latitude of the subsolar point during equinoxes) and decreases toward higher latitudes along with the noontime solar angle, as expected for an *in situ* forced tide. NRLMSISE-00 does not include nonmigrating tides. Recent diagnostics of upper thermosphere neutral density observations from the CHAllenging Minisatellite Payload (CHAMP) satellite indicate that nonmigrating tides induce an additional longitudinal variability on the order of 30–50%, mostly due to upward-propagating tides from the troposphere. An accurate description of migrating and nonmigrating diurnal density variations is especially important for predicting low perigee satellite trajectories because atmospheric drag is the dominant error source in operational models.

Nonmigrating Tides

Near the surface of the Earth the strong longitudinal differences in topography, land–sea contrast, and surface interactions produce zonal (i.e., along a latitude circle in the east–west direction) variations in the local time behavior of the atmosphere and thus excite nonmigrating tides. A good example is latent heat release due to condensation in large-scale deep convective systems in the tropical troposphere. Figure 6 illustrates the latitude–longitude distributions of the diurnal (left) and semidiurnal (right) latent heat release amplitudes during the month of September derived from satellite-borne convective rainfall measurements. Both components maximize at low latitudes where the absorption of solar radiation (evaporation) is greatest. Their longitudinal structure reflects the areas of largest deep convective activity in the tropical troposphere: one peak over Africa, followed by two peaks over Indonesia and the western Pacific and a fourth over South and Central America.

Through Fourier analysis the longitude variations depicted in Figure 6 may be decomposed into a series of wave components with different zonal wavenumbers *s*. Each of the resultant nonmigrating tidal components possesses different vertical propagation characteristics that depend on its sensitivity to the prevailing winds and its vertical wavelength. Good examples are the DW5 and DE3 components. Both are efficiently forced by latent heat release but DW5 dissipates at higher altitudes due to its short vertical wavelength. DE3 on the other hand has a long vertical wavelength and propagates up into the lower thermosphere where its magnitude rivals the radiatively forced migrating diurnal tide (Movie 2).

It is difficult to track vertical tidal propagation into the upper atmosphere such as that depicted in Movie 2 because the distribution of ground-based observations is spatially limited. This is particularly true for altitudes between about 30 and 180 km above the Earth's surface, which encompass the region where the upward-propagating waves attain large amplitudes and subsequently dissipate. It is generally impossible to distinguish migrating from nonmigrating tides in the analysis of ground-based remote-sensing measurements from a single site made at these altitudes. During the 1990s remote sensing from the Upper Atmosphere Research Satellite (UARS) considerably ameliorated this problem. Further progress came from the Thermosphere Ionosphere Mesosphere Energetics and Dynamics (TIMED) satellite that was launched in 2001 because it allowed for the first time to observe the global tidal spectrum in various parameters over a range of mesosphere and lower thermosphere altitudes. The data utilized to construct Movies 1–4 consist of wind measurements made by the TIMED Doppler Interferometer (TIDI) and temperature measurements made by the Sounding the Atmosphere using Broadband Emission Radiometry instrument that are extended toward the poles and into the lower atmosphere and upper thermosphere using an empirical tidal model.

Movies 3 and 4 illustrate the latitude–longitude distribution of the diurnal and semidiurnal tides at 100 km for the month of September, averaged over 7 years from 2002 to 2008. The superposition of these movies is shown in Movie 1. The diurnal tide with amplitudes as large as 28 K and 42 $\mathrm{m\,s^{-1}}$, respectively, mainly consists of the migrating component DW1 and the nonmigrating DE3 tide, with some contributions from the DE2, D0, and DW2 components. The migrating tide is observed as a zonally symmetric oscillation because the movie is animated in LT (compare eqn [5]) and the DE3 as a 4-peaked longitudinal variation for the same reason. The semidiurnal tidal field is more symmetric than the diurnal one with amplitudes of 17 K and 36 $\mathrm{m\,s^{-1}}$, respectively. Spectral analysis of these particular data reveals that the longitudinal structure is dominated by the migrating tide SW2, with contributions from the SW3, SW1, and SE2 nonmigrating tides.

Complementary numerical modeling studies suggest that the diurnal and semidiurnal nonmigrating tides are

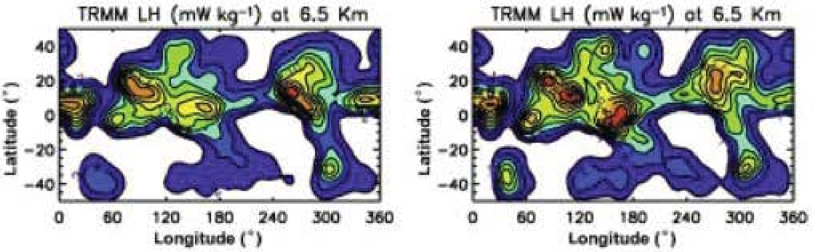

Figure 6 Contours of diurnal (left) and semidiurnal (right) latent heat release amplitudes in the troposphere from Tropical Rainfall Measuring Mission (TRMM) satellite observations during September. Dr X. Zhang provided these figures, which are adapted with permission from Zhang, X., J.M., Forbes, M.E., Hagan, 2010. Longitudinal variation of tides in the MLT region: 2. Relative effects of solar radiative and latent heating. Journal of Geophysical Research 115, A06317. doi:10.1029/2009JA014898.

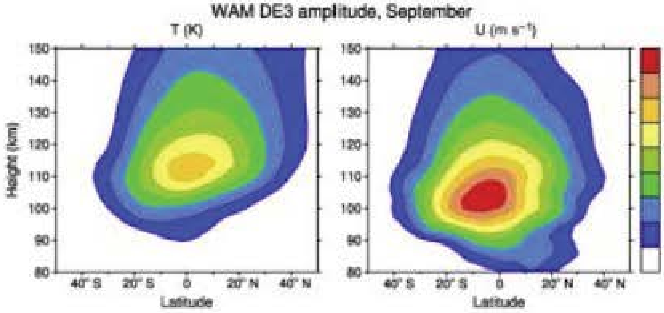

Figure 7 WAM DE3 amplitude of (left) temperature and (right) zonal wind as a function of latitude and height in September. Dr R.A. Akmaev provided the model results, which are adapted with permission from Akmaev, R.A., T.J., Fuller-Rowell, F., Wu, J.M., Forbes, X. Zhang, A.F., Anghel, M.D., Iredell, S., Moorthi, H.-M., Juang, 2008. Tidal variability in the lower thermosphere: comparison of whole atmosphere model (WAM) simulations with observations from TIMED. Geophysical Research Letters 35, L03810, doi:10.1029/2007GL032584.

generated in the lower levels of the atmosphere, either by latent heat release (DE3, DE2, SE2) and/or as secondary waves by the nonlinear interaction between stationary planetary waves and the migrating tides (DW2, D0, SW1, SW3). An example from the 'Whole Atmosphere Model' (WAM) is shown in Figure 7. WAM is a general circulation model of the neutral atmosphere built on an existing operational Global Forecast Model used by the U.S. National Weather Service. It includes realistic topography, latent heating associated with tropospheric convection and nonlinear processes, and the model domain extends well into the dissipative thermosphere to a top level of about 600 km. The WAM temperature and zonal wind components associated with the DE3 tide exhibit maxima centered around the equator that can also be discerned in the TIMED satellite measurements shown in Movie 2.

Lunar Tides

Lunar atmospheric tides are only about 5–10% as large as solar tides, but they have clearly detectable effects. The lunar tidal pressure at the ground maximizes at low latitudes, with an average amplitude of about 7 Pa. The corresponding wind amplitude at the Equator is about 0.03 m s^{-1}. The wind amplitude increases with altitude up to about 110 km, where it reaches an amplitude on the order 10 m s^{-1}.

Unlike the solar tides, the lunar atmospheric tides are entirely driven by gravitational forces, as illustrated schematically in Figure 8. Because the lunar gravitational acceleration decreases as the inverse square of the distance from the center of the Moon, this acceleration is not exactly uniform near the Earth, so that atmospheric air parcels at various locations around the Earth experience slightly different lunar accelerations from those of the Earth as a whole. Air parcels in the hemisphere most distant from the Moon are accelerated toward the Moon less strongly than is the Earth, in effect creating a relative acceleration away from the Moon for these air parcels, in the Earth's reference frame. Conversely, air parcels in the moonward hemisphere of the Earth experience a relative acceleration toward the Moon. In each hemisphere, parcels to the west of a line passing through the centers of the Earth and Moon experience an eastward component of acceleration, while those to the east of this line experience a westward acceleration. As the Earth rotates, during a lunar day (24.8412 h on the average) an air parcel at the Equator successively passes twice through regions of westward and eastward acceleration, comprising two lunar semidiurnal cycles of period 12.4206 h. When the Moon is north or south of the Earth's Equator, an additional diurnal lunar cycle (period 24.8412 h) of acceleration exists at nonequatorial latitudes. There is also a monthly periodicity to the forcing as the Moon cycles between the Northern and Southern Hemispheres of the Earth. Both this cycling and the ellipticity of the Moon's orbit create amplitude and frequency modulation of the lunar semidiurnal and diurnal forcings that can be expressed as combinations of multiple closely spaced periods. The dominant lunar period, representing the average lunar semidiurnal tide, is referred to as the M2 tide, with a 12.4206 h period.

In addition to the direct forcing of lunar gravity on the atmosphere, lunar atmospheric tides are indirectly forced by

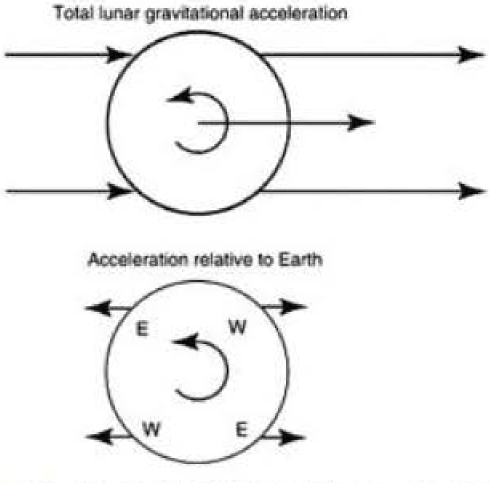

Figure 8 Schematics of lunar tidal forcing in the reference frames of the Moon (top) and the Earth (bottom). The Earth is viewed from above the North Pole and the Moon (not shown) is to the right.

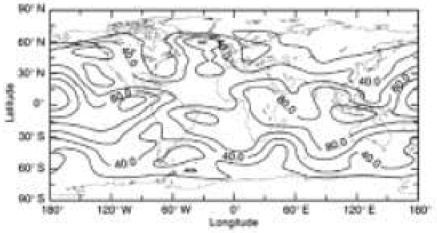

Figure 9 Contours of M2 lunar semidiurnal surface pressure amplitude (dPa) against longitude and latitude for the month of December. Dr F. Vial collaborated with Professor J.M. Forbes to produce the model results.

lunar gravity through deformation of the Earth's surface due to ocean and Earth tides. The vertical velocity associated with this deformation significantly affects the atmospheric tide, and the modulation of terrestrial gravity by the deformation of the Earth's mass distribution also has an effect. These indirect forcing effects can be determined accurately from measurements of ocean and Earth tides, so that the total lunar tidal forcing is well known. This is beneficial for testing theoretical models of tidal propagation and dissipation in the atmosphere. The indirect forcing effects, because they depend on land–sea differences, are a function not only of apparent lunar position but also of geographical location, and generate nonmigrating tides in addition to the primary migrating lunar tides.

It is possible to develop a model of the M2 lunar semidiurnal atmospheric tide that produces results that agree very satisfactorily with the observed tide in the surface pressure. Such a model must account for all direct and indirect lunar forcing effects, and include realistic atmospheric wind and temperature structures. Figure 9 illustrates prototypical M2 model results and shows how the lunar tidal amplitude varies with latitude and longitude over the Earth for atmospheric conditions representing the month of December. The largest amplitudes in this month are at low latitudes, but they vary from less than 4 Pa (40 dPa) on the east coast of South America to more than 12 Pa over the mid-Pacific. A secondary maximum appears over the northern Atlantic. On the average, the amplitude of the M2 tide at low latitudes is larger around the solstices than at the equinoxes, by roughly 50%. Some of the largest geophysical effects of atmospheric lunar tides appear in the low-latitude ionosphere, as discussed in the next section.

Tides in the Ionosphere

Tides in the ionosphere are spatiotemporal variations in electric fields, currents, and plasma density in the ionosphere primarily due to dynamo effects generated by solar and lunar tidal motions in the neutral background atmosphere. Tidal winds in the low and middle latitude E-region move the partially ionized plasma through the Earth's magnetic field while the electrons with their high gyro frequency/collision frequency ratio remain fixed to the magnetic field lines. An electromotive force is thus created with ensuing electric currents and polarization electric fields.

During the daytime, when the conductivity is large owing to ionizing solar radiation, the electric currents, commonly labeled S_q for 'solar quiet,' flow approximately counter clockwise in the Northern Hemisphere and clockwise in the Southern Hemisphere with vortex foci at roughly ±30° magnetic latitude. A particularly strong eastward current, called equatorial electrojet, exists along the geomagnetic equator because the effective ionospheric conductivity is unusually high in the lower ionosphere at latitudes where the geomagnetic field is nearly horizontal. The S_q currents produce perturbations in the Earth's magnetic field that are readily measured at the ground. Figure 10 shows the northward component of the magnetic perturbation at Huancayo, Peru, for two phases of the lunar tide: 5 and 12 days following new moon. These represent average conditions in 1957–58 for the months of November–February, when the lunar tide in the ionosphere is generally largest. The larger solar diurnal and semidiurnal tides produce a northward perturbation that maximizes daily at around 11.00 LT. On day 5, the lunar tide enhances the magnetic perturbation at 11.00 LT, but reduces it in the late afternoon. On day 12 the phase of the lunar tide and its effects are reversed from those on day 5. Clear lunar effects in the low-latitude ionospheric electron density are also found.

The E-region dynamo polarization electric fields are further transmitted along magnetic field lines into the overlying F-region where they drive vertical ($\sim 20\ \mathrm{m\ s^{-1}}$) and zonal ($\sim 100\ \mathrm{m\ s^{-1}}$) plasma drifts, which influence many important ionospheric processes. For example, vertical ExB drifts drive the plasma fountain which results in dense bands of plasma

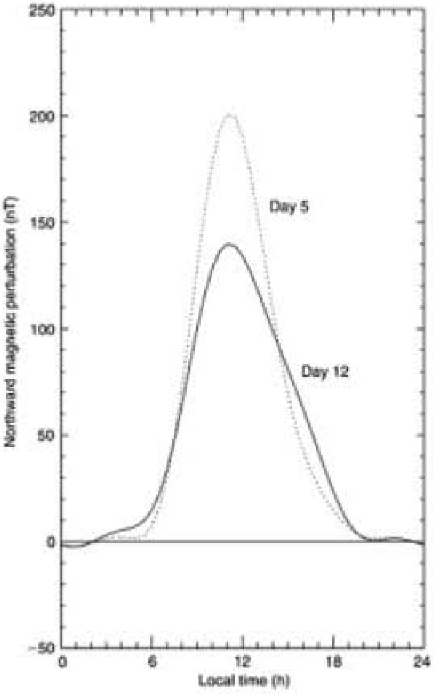

Figure 10 The northward component of magnetic perturbation (in nanoteslas) at Huancayo, Peru, against local time (h) on the 5th and 12th days following new moon reveals evidence of lunar tidal effects on top of the larger solar tidal effects.

centered near ±15–20° magnetic latitude. This so-called equatorial ionization anomaly can be seen in the top center panel in Figure 11, as the two bluish bands north and south of the magnetic equator. The two ionization crests are predominantly the result of migrating solar tidal winds in the E-region while the apparent longitudinal modulation on top, indicated by brighter colors, is the result of nonmigrating tides excited in the troposphere by latent heat release in deep convective tropical clouds.

The realization that nonmigrating tides due to tropospheric weather impact the F-region ionosphere, and as such couple these atmospheric layers that are 400 km apart, is a relatively new discovery that was made around the year 2005 due to new satellite observations and progress in numerical modeling. Figure 11 summarizes these observations that are all displayed for a constant LT, and sketches the cause-and-effect chain of meteorological impacts on the IT system. The most striking pattern is a 4-peaked 'wave-4' longitudinal modulation that is apparent in deep convective cloud occurrence (observed by weather satellites, also compare Figure 6), E-region zonal winds (observed by TIMED, also compare Movie 1), thermospheric constituents (observed by the SNOE in equatorial nitric oxide density), electron density (observed by the COSMIC/Formosat-3), ion density (observed by IMAGE spacecraft in the far-ultraviolet), and neutral mass density (observed by CHAMP). The 'wave-4' corresponds to the DE3 nonmigrating tide with some contribution from the SE2, because this is how these components are observed in a LT frame (eqn [5]). Movie 2 and Figure 6 show that the DE3 can achieve zonal wind amplitudes on the order of tens of m s^{-1} in the low latitude E-region. It thus efficiently modulates the E-region dynamo electric fields, resulting in the pronounced 'wave-4' F-region plasma density variations. All these observations and corresponding model simulations imply that tropospheric weather is an important contributor to the 'space weather' of the geomagnetically quiescent ionosphere, even for solar maximum conditions, and capable to change, for example, electron density by a factor of three within a few thousand kilometers.

Longitudinal variations in the ionospheric plasma due to nonmigrating tides do not always occur as a 'wave-4.' The 'wave-4' dominates from March to October but changes to a 3-peaked 'wave-3' from November to February when observed at a fixed LT (Figure 12). This is mainly due to the seasonal variation of the diurnal nonmigrating tides in the E-region as depicted in Figure 13. The DE3 dominates from March to October but it is exceeded by another component, the DE2 (observed as a 'wave-3') during Northern Hemisphere winter.

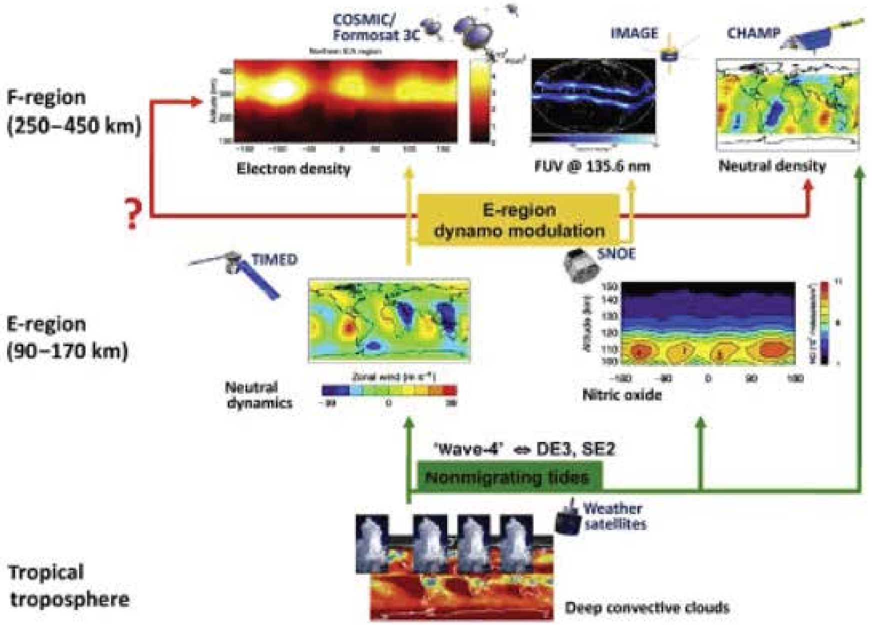

Figure 11 Meteorological impacts on the ionosphere–thermosphere due to nonmigrating tides as observed by different satellites. The 'wave-4' like latent heat release pattern in the troposphere is found throughout the ionosphere–thermosphere system in various neutral and ion parameters. Dr C.H. Lin provided the Constellation Observing System for Meteorology, Ionosphere & Climate (COSMIC) figure, which is adapted with permission from Lin, C.H., et al., 2007. Plausible effect of atmospheric tides on the equatorial ionosphere observed by the FORMOSAT-3/COSMIC: three-dimensional electron density structures. Geophysical Research Letters 34, L11112. doi:10.1029/2007GL029265. Dr T.J. Immel provided the IMAGE figure, which is adapted with permission from Immel, T.J., et al., 2006. Control of equatorial ionospheric morphology by atmospheric tides. Geophysical Research Letters 33, L15108. doi:10.1029/2006GL026161. Dr X. Zhang and Dr S.L. Bruinsma provided the CHAMP neutral density data. The Student Nitric Oxide Explorer (SNOE) nitric oxide figure is adapted with permission from Oberheide, J., Forbes, J.M., 2008. Thermospheric nitric oxide variability induced by nonmigrating tides. Geophysical Research Letters 35, L16814. doi:10.1029/2008GL034825. Deep tropical cloud data are from the International Satellite Cloud Climatology Project (ISCCP).

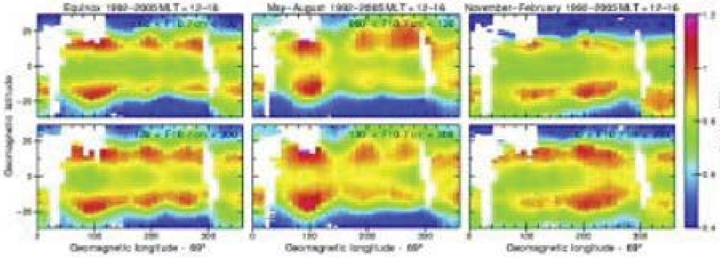

Figure 12 Seasonal variation of normalized total electron content from TOPEX/Poseidon observations for low (upper row) and high (lower row) solar flux conditions. Professor L. Scherliess provided these figures, which are adapted with permission from Scherliess, L., Thompson, D.C., Schunk, R.W., 2008. Longitudinal variability of low-latitude total electron content: tidal influences. Journal of Geophysical Research 113, A01311. doi:10.1029/2007JA012480.

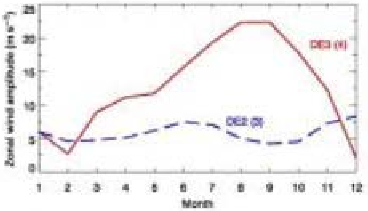

Figure 13 Seasonal variation of the DE2 and DE3 zonal winds at the equator and 105 km as observed by the TIDI/TIMED instrument. The numbers in parentheses indicate the zonal wavenumbers when observed in a LT frame.

The leading role of E-region dynamo modulation in coupling tidal dynamics into the ionosphere is undisputed but there is growing evidence that other processes may play an important role. While *in situ* F-region ion drag has no measureable effect on the neutral 'wave-4' in the upper thermosphere, models on the other hand suggest that tidal variations in thermospheric [O]/[N$_2$] and meridional winds at F-region altitudes may add to the observed plasma variations, including effects from semidiurnal nonmigrating tides such as the SE2. Delineating and understanding these processes, including nonlinear wave–wave interactions and secondary wave generation, is one challenge for the time to come as tidal coupling from below constitutes a major energy term for the ionosphere–thermosphere system. It is particularly important since it is a prerequisite for improved space weather predictions including Global Positioning System outages due to ionospheric irregularities or biteouts.

Appendix A: Supplementary Data

Supplementary video related to this article can be found at http://dx.doi.org/10.1016/B978-0-12-382225-3.00409-6.

The following are the supplementary data related to this article:

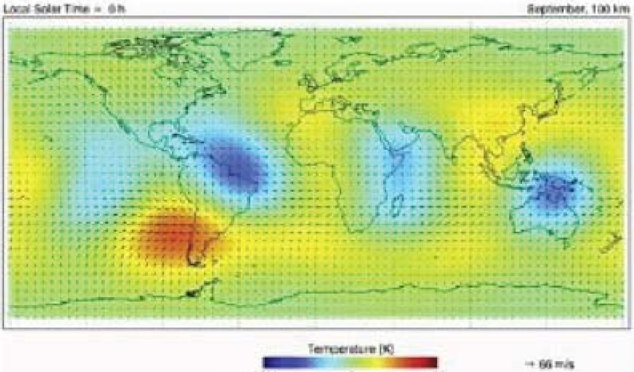

Movie 1 Temperature (color) and wind variations (arrows) at 100 km during September due to diurnal and semidiurnal solar atmospheric tides. The movie is based on TIMED satellite observations and runs in local solar time (LT).

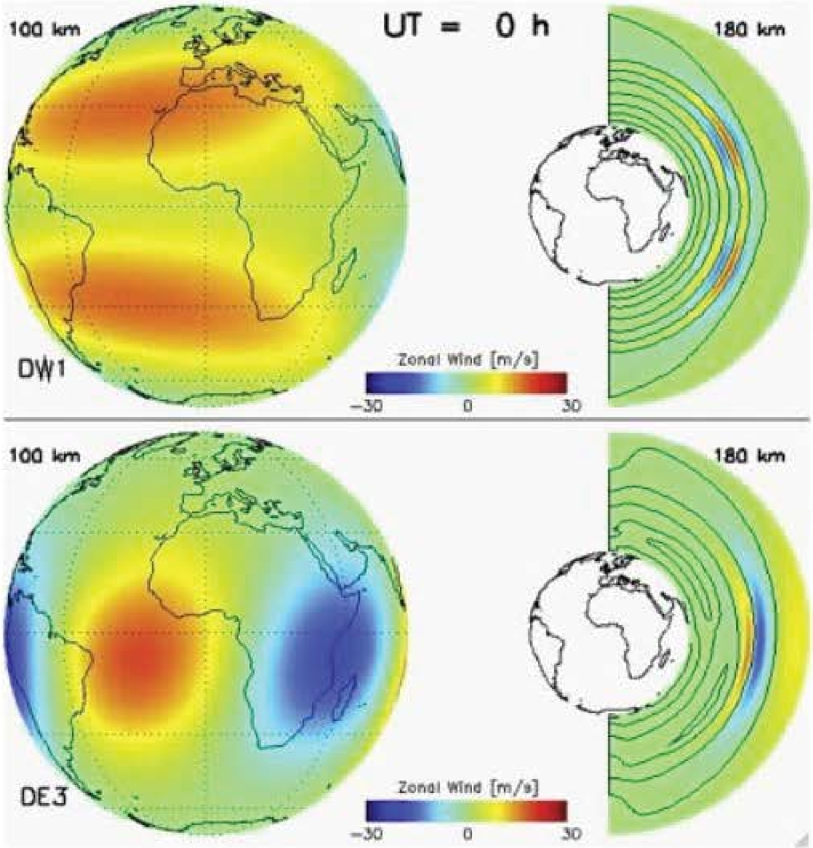

Movie 2 Zonal wind structure of the migrating diurnal tide (DW1, top) and the eastward propagating nonmigrating tide of zonal wavenumber 3 (DE3, bottom). The movie is based on TIMED satellite observations and empirical modeling and runs in universal time. The right column shows the vertical structure of the tides at 90° E longitude. Downward phase progression indicates tidal forcing from below. Thermospheric tides due to far and extreme ultraviolet absorption are not included.

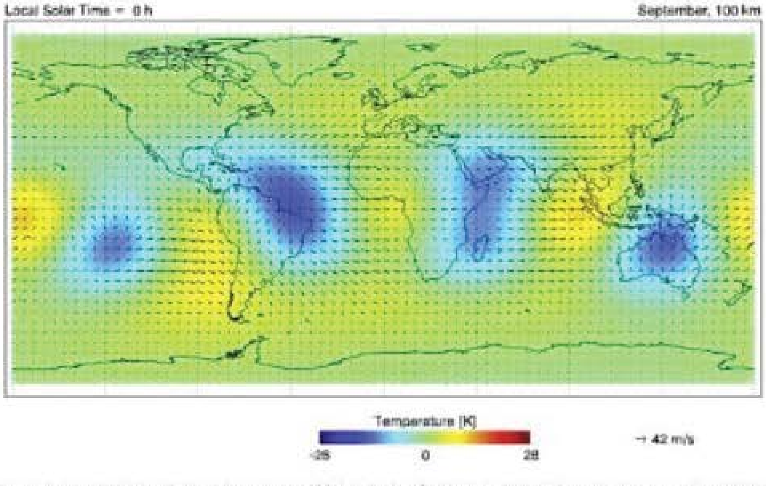

Movie 3 Temperature (color) and wind variations (arrows) at 100 km during September due to diurnal solar atmospheric tides. The movie is based on TIMED satellite observations and runs in LT.

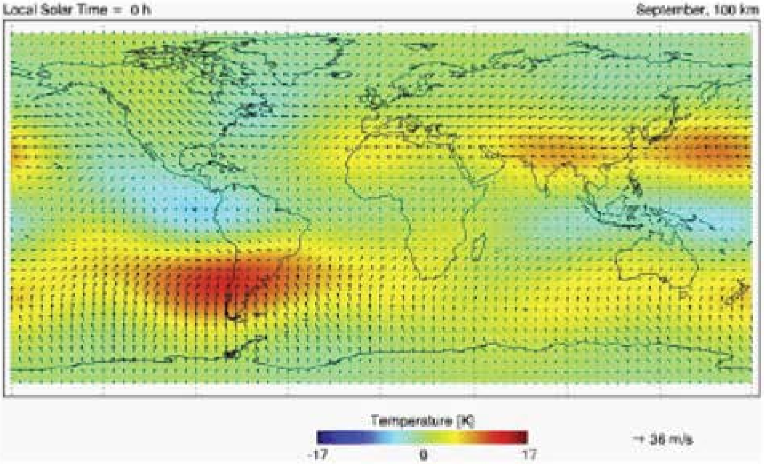

Movie 4 As Movie 3 but for the semidiurnal tide.

See also: **Boundary Layer (Atmospheric) and Air Pollution:** Diurnal Cycle. **Gravity Waves:** Buoyancy and Buoyancy Waves: Optical Observations; Buoyancy and Buoyancy Waves: Theory; Overview. **Mesosphere:** Ionosphere. **Numerical Models:** Parameterization of Physical Processes: Gravity Wave Fluxes. **Radar:** Meteor Radar.

Acknowledgment

The authors thank Hanli Liu for comments on an initial draft of the article. The National Center for Atmospheric Research is sponsored by the National Science Foundation.

Further Reading

Akmaev, R.A., Fuller-Rowell, T.J., Wu, F., Forbes, J.M., Zhang, X., Anghel, A.F., Iredell, M.D., Moorthi, S., Juang, H.-M., 2008. Tidal variability in the lower thermosphere: comparison of whole atmosphere model (WAM) simulations with observations from TIMED. Geophysical Research Letters 35, L03810. http://dx.doi.org/10.1029/2007GL032584.

Chapman, S., Bartels, J., 1940. Geomagnetism. Clarendon Press, Oxford.

Chapman, S., Lindzen, R.S., 1970. Atmospheric Tides. Reidel, Dordrecht.

Dai, A., Wang, J., 1999. Diurnal and semidiurnal tides in global surface pressure fields. Journal of Atmospheric Sciences 6, 3874–3891.

England, S.L., Immel, T.J., Huba, J.D., Hagan, M.E., Maute, A., DeMajistre, R., 2010. Modeling of multiple effects of atmospheric tides on the ionosphere: an examination of possible coupling mechanisms responsible for the longitudinal structure of the equatorial ionosphere. Journal of Geophysical Research 115, A05308. http://dx.doi.org/10.1029/2009JA014894.

Forbes, J.M., 1995. Tidal and planetary waves. Geophysics Monographs 87, 67–87.

Hagan, M.E., Forbes, J.M., Vial, F., 1995. On modeling migrating solar tides. Geophysical Research Letters 22, 893–896.

Hagan, M.E., Maute, A., Roble, R.G., Richmond, A.D., Immel, T.J., England, S.L., 2007. Connections between deep tropical clouds and the Earth's ionosphere. Geophysical Research Letters 34, L20109. http://dx.doi.org/10.1029/2007GL030142.

Haurwitz, B., Cowley, A.D., 1973. The diurnal and semidiurnal oscillations, global distribution and annual variation. Pure and Applied Geophysics 102, 193–222.

Immel, T.J., Sagawa, E., England, S.L., Henderson, S.B., Hagan, M.E., Mende, S.B., Frey, H.U., Swenson, C.M., Paxton, L.J., 2006. Control of equatorial ionospheric morphology by atmospheric tides. Geophysical Research Letters 33, L15108. http://dx.doi.org/10.1029/2006GL026161.

Lin, C.H., Wang, W., Hagan, M.E., Hsiao, C.C., Immel, T.J., Hsu, M.L., Liu, J.Y., Paxton, L.J., Fang, T.W., Liu, C.H., 2007. Plausible effect of atmospheric tides on the equatorial ionosphere observed by the FORMOSAT-3/COSMIC: three-dimensional electron density structures. Geophysical Research Letters 34, L11112. http://dx.doi.org/10.1029/2007GL029265.

Liu, H., Yamamoto, M., Lühr, H., 2009. Wave-4 pattern of the equatorial mass density anomaly: a thermospheric signature of tropical deep convection. Geophysical Research Letters 36, L18104. http://dx.doi.org/10.1029/2009GL039865.

Matsushita, S., 1967. Solar quiet and lunar daily variation fields. In: Matsushita, S., Campbell, W.H. (Eds.), Physics of Geomagnetic Phenomena. Academic Press, New York, pp. 301–427.

Matsushita, S., 1967. Lunar tides in the ionosphere. In: Handbuch der Physik. Springer-Verlag, Berlin, pp. 547–602.

Oberheide, J., Forbes, J.M., 2008. Thermospheric nitric oxide variability induced by nonmigrating tides. Geophysical Research Letters 35, L16814. http://dx.doi.org/10.1029/2008GL034825.

Oberheide, J., Forbes, J.M., Zhang, X., Bruinsma, S.L., 2011. Wave-driven variability in the ionosphere–thermosphere–mesosphere system from TIMED observations: what contributes to the "wave-4"? Journal of Geophysical Research 116, A01306 http://dx.doi.org/10.1029/2010JA015911.

Picone, J.M., Hedin, A.E., Drob, D.P., Aikin, A.C., 2002. NRLMSISE-00 empirical model of the atmosphere: statistical comparison and scientific issues. Journal of Geophysical Research 107 (A12), 1468. http://dx.doi.org/10.1029/2002JA009430.

Richmond, A.D., 1995. The ionospheric wind dynamo: effect of its coupling with different atmospheric regions. In: Johnson, R.M., Killeen, T.L. (Eds.), The Upper Mesosphere and Lower Thermosphere: A Review of Experiment and Theory, Geophysical Monograph 87. American Geophysical Union.

Scherliess, L., Thompson, D.C., Schunk, R.W., 2008. Longitudinal variability of low-latitude total electron content: tidal influences. Journal of Geophysical Research 113, A01311. http://dx.doi.org/10.1029/2007JA012480.

Vial, F., Forbes, J.M., 1994. Monthly simulations of the lunar semi-diurnal tide. Journal of Atmospheric and Solar-Terrestrial Physics 56, 1591–1607.

Vincent, R.A., Kovalam, S., Fritts, D.C., Isler, J.R., 1998. Long-term MF radar observations of solar tides in the low-latitude mesosphere: interannual variability and comparisons with the GSWM. Journal of Geophysical Research 103, 8667–8683.

Volland, H., 1988. Atmospheric Tidal and Planetary Waves. Kluwer Academic, Dordrecht.

Zhang, X., Forbes, J.M., Hagan, M.E., 2010. Longitudinal variation of tides in the MLT region: 2. Relative effects of solar radiative and latent heating. Journal of Geophysical Research 115, A06317. http://dx.doi.org/10.1029/2009JA014898.